Aeroelastic Modeling of Hose and Drogue Aerial Refueling Systems Including a Hose Reeling Mechanism

Andrew J. Erickson[1], Phillip W. Richards[2], Arnav N. Chaturvedi[3]
SDI Engineering Inc., Kirkland, Washington, 98033

Elizabeth Knoblauch[4], Steve McLaughlin[5]
NAVAIR

U.S. Navy aerial refueling operations commonly utilize a hose-and-drogue system to connect a receiver to a tanker aircraft. For pilot training, it is important to have a physics-based simulation of the hose and drogue system, so that pilots are able to practice aerial refueling with realistic hose and drogue behavior in a flight simulator. A modeling, simulation and analysis software package called ARES (Aerial Refueling Simulation) has been developed to study the aeroelastic behavior of the hose and drogue during aerial refueling events. ARES has been developed in a MATLAB/Simulink environment and utilizes a detailed modeling approach for each of the relevant subsystems, including the hose, drogue and reeling mechanism. This paper introduces the ARES approach, describes the validation efforts that have been undertaken, and provides a brief analysis of the hose aeroelastic response.

I. Nomenclature

A	=	Projected frontal area
AR	=	Aerial Refueling
ARES	=	Aerial Refueling Simulation
c	=	Linear damping coefficient
C_D	=	Drag coefficient
C_L	=	Lift coefficient
D	=	Drag force
F	=	Force
FFT	=	Fast Fourier Transform
I	=	Moment of inertia
k	=	Linear stiffness coefficient
KCAS	=	Knots, Calibrated Air Speed
L	=	Lift
MFS	=	Manned Flight Simulator
NAVAIR	=	Naval Air Systems Command
ORS	=	Optical Reference System
R	=	Radius
Re	=	Reynolds number
SDI	=	SDI Engineering Inc.
T	=	Torque
U	=	Airspeed

[1] Principal Aeronautical Engineer, aerickson@sdi-eng.com, AIAA Member
[2] Principal Aeronautical Engineer, prichards@sdi-eng.com, AIAA Member
[3] Aeronautical Engineer, achaturvedi@sdi-eng.com
[4] Engineer, elizabeth.knoblauch@navy.mil
[5] Senior Engineer, steve.mclaughlin@navy.mil

α	=	Angle of attack
ρ	=	Density
θ	=	Relative angle between adjacent hose elements
$\dot{\theta}$	=	Relative angular velocity between adjacent hose elements
$\ddot{\theta}$	=	Relative angular acceleration between adjacent hose elements
ω	=	Natural bending frequency
ζ	=	Bending damping coefficient

II. Introduction and Background

This paper introduces ARES, an engineering analysis software toolbox developed by SDI Engineering Inc. to analyze the dynamics of aerial refueling (AR) hoses. ARES is based in MATLAB/Simulink and uses Simscape Multibody to model each of the flexible structures and simulate the dynamics of the aerial refueling hose and drogue system. The MATLAB/Simulink environment also allows easy integration with 3rd party software for the purpose of operations support, flight controls evaluation, pilot-in-the-loop analysis and pilot training.

The ARES toolset is currently being developed and validated in a Small Business Innovation Research (SBIR) effort in collaboration with the U.S. Navy Naval Air Systems Command (NAVAIR). NAVAIR desires to improve the accuracy and computational efficiency of their hose and drogue simulations, for real-time use in manned flight simulators (MFS). It is important to have a physics-based simulation of the hose and drogue system, so pilots are able to practice aerial refueling with realistic hose and drogue behavior and hose reel response throughout all phases of the aerial refueling event.

Aerial refueling hoses are long, slender bodies with low bending stiffness. If the bending stiffness is neglected, and tension is assumed to be the only structural reaction force, then the hose may be modeled as a vibrating string. If bending stiffness is considered, then a beam-like approach may be taken instead. In either case, the speed of a wave's propagation is related to the vibration frequencies, so it can be imagined that capturing the proper vibration frequencies of the hose may be critical to accurate prediction of the hose aeroelastic behavior.

A common approach towards modeling the hose is to treat it as a catenary, neglect the bending stiffness of the hose, and model only the tension effects. In this method, the hose is discretized into nodes, the distance between each node is measured and a tension is applied along the line of action between the two nodes. However, this method provides inaccurate results when hose tension is low and becomes singular as the cable tension drops to zero (Ref. [1]). The catenary approach assumes the cable tension is several orders of magnitude higher than its bending and torsional moments. However, in a low-tension cable, the mechanism of energy propagation is dominated by bending rather than string tension. Thus, the bending stiffness of the hose cannot be safely neglected (Ref. [2], [3]).

Many aerial refueling models utilize a method originally developed by Ribbens et al. that uses the vibrating string nodal approach and adds an equivalent hose bending force to represent the bending stiffness of the hose (Ref. [4]). Boothe et al. extended this method to 3D, which is the basis for NAVAIR's current aerial refueling model (Ref. [5]).

This paper introduces an element-based multibody dynamics approach to modeling the hose. In this approach, the hose is divided into rigid body elements which are connected using spring and damper elements to represent axial and bending stiffness and damping. The spring elements are linear springs to represent tension, and torsion springs to represent bending. The rigid body elements are also subjected to aerodynamic lift and drag. The hose model stiffnesses were determined through dynamic tests of the hose structural properties.

The investigation of the effects of a hose reeling system on the hose aeroelastic behavior is also presented. In a typical aerial refueling event, the receiver approaches the drogue at a closure rate of 1-5 knots. After the probe-drogue engagement, the drogue is driven forward, reducing the hose tension and allowing slack to develop in the hose. This increases the angle of attack of the hose, which increases the lift and drag forces, inducing a transverse wave that travels up the hose to the tanker and reflects back to the probe-drogue connection. In certain conditions, this can produce loads that may cause the drogue to disconnect from the probe or even damage the drogue and probe (Ref. [4]). The hose reeling system is designed to take up this slack, reduce the hose whip dynamic behavior and thus reduce the loads experienced by the drogue and probe. Simulations of hose aeroelastic response with and without a hose reel are compared.

Finally, flight test data from aerial refueling events has been compared to the toolset's predictions in order to validate the hose and drogue static and dynamic behavior. These validation efforts are described and the preliminary results and predictions of the hose aeroelastic behavior are discussed.

III. Refueling Hose and Drogue Modeling

The components of the aerial refueling system covered in this paper include the hose, the drogue, and the hose reel system.

A. Hose Structural Equations of Motion

The ARES software developed by SDI takes a lumped-parameter approach for modeling the hose. The hose is divided into rigid body elements, and these are connected using spring and damper elements. The spring elements are linear springs to represent tension and torsion springs to represent bending. This approach was initially verified by comparing results for the hose deflection under various loading conditions against NASTRAN's linear and nonlinear analysis capabilities. A basic diagram of the hose elements connected in series is shown in Fig. 1.

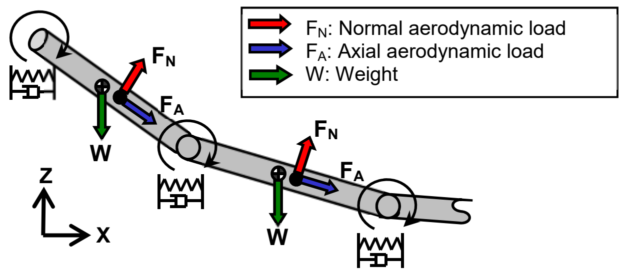

Fig. 1 Simscape Multibody hose model illustration

Each hose element consists of two rigid bodies coupled by springs and dampers. The elongation (x) and rotation angle (θ) of the n^{th} generalized hose element executes damped motion according to the force and moment equations given by:

$$\boldsymbol{\Sigma F = m\ddot{x}_n + c\dot{x}_n + kx_n} \tag{1}$$

$$\boldsymbol{\Sigma M/I = \ddot{\theta}_n + 2\zeta\omega_0\dot{\theta}_n + \omega_0^2\theta_n} \tag{2}$$

where k is the axial stiffness, c is the axial damping coefficient, $\boldsymbol{\omega_0}$ is the natural bending frequency, and $\boldsymbol{\zeta}$ is the bending damping coefficient. Because the hose is constructed from a combination of steel and rubber, and due to the viscoelastic nature of rubber, it is not straightforward to calculate the stiffness and damping terms from the material properties and geometry.

B. Hose Property Testing

SDI, in partnership with Moog CSA Engineering (Moog CSA), conducted tests to determine the stiffness and damping characteristics of the several aerial refueling hoses. NAVAIR provided Moog CSA with sample sections of a retired KC-130 "long hose" and F/A-18 E/F "Buddy Store" hose. Moog CSA performed the tests described in this section to measure the acceleration response of the end of the hose section in both bending and axial extension. The KC-130 "long hose" and F/A-18 "Buddy Store" hose stiffness and damping properties were then tuned to this dataset.

The dynamic stiffness and damping hose tests measured the acceleration response of the hose section to an excitation in both the axial and bending directions. The frequency and rate of decay of the first structural mode of the hose in each direction were used to estimate stiffness and damping properties for the hose material.

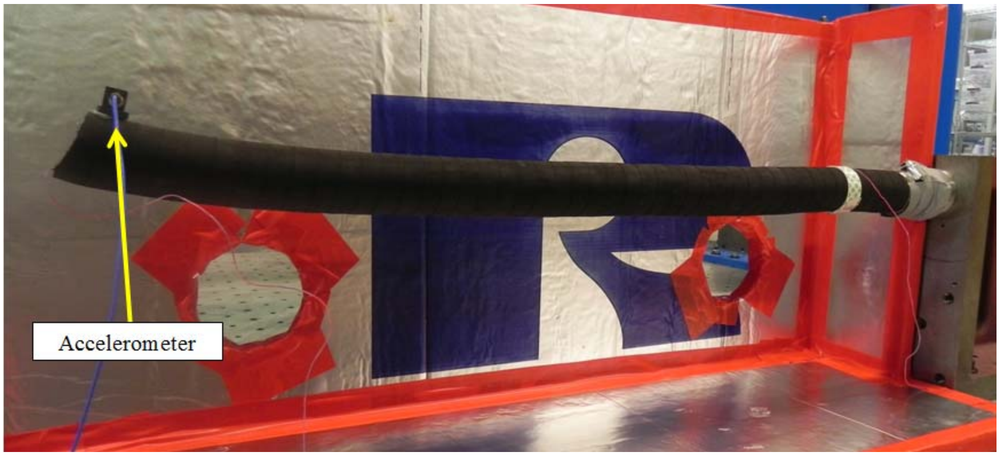

Fig. 2 Hose section mounted in bending test configuration

The bending stiffness test was performed with the hose section mounted in a cantilever arrangement with one of its ends fixed and the other free, as shown in Fig. 2. The dynamic response of the hose was measured using an accelerometer fixed to the free end. A thermal enclosure was built around the hose section to allow the bending stiffness test to be performed at multiple temperatures, thus allowing a study of the variation of stiffness and damping with temperature. Thermocouples on each end of the hose verified the temperature of the hose material during each test. The bending tests were performed at six temperatures: 60 °F, 40 °F, 20 °F, 0 °F, -20 °F, and -50 °F. The hose section was excited by displacing the tip of the hose downward and then releasing it, allowing the hose to "ring down" to its neutral state. This input primarily excited the first bending mode of the hose.

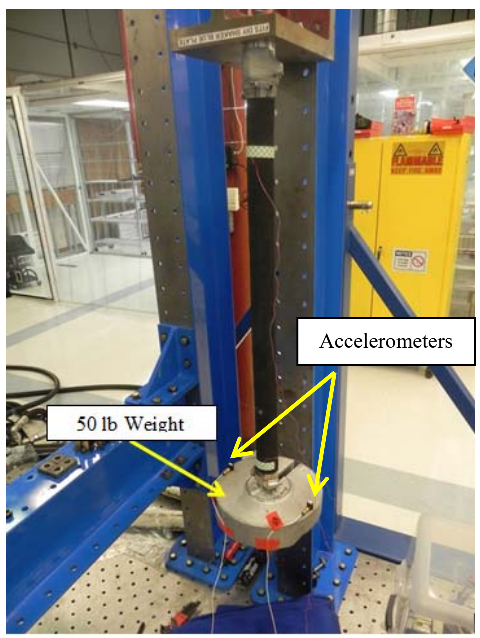

Fig. 3 Hose section mounted in the axial test configuration

The axial stiffness test was performed with the "Buddy Store" hose section hung from a fixed boundary condition as shown in Fig. 3. A weight was fixed to the end of the hose to prevent the hose section from curling up, since the hose section had set into a curve while in storage. The weight was instrumented with two accelerometers placed on opposite sides at an equal distance from the hose centerline. These accelerometers were used to determine the difference between the rocking and axial motion. To excite the hose, a stud on the underside of the weight was struck with a hammer. The hose response to this input was captured by the accelerometers until the hose section came to rest. The temperature was not varied in the axial configuration because the thermal enclosure was unable to be fitted to the axial configuration test stand. Rather, the temperature dependent trends captured in the bending test data reduction were applied to the data from the axial stiffness test.

Fig. 4 shows an example of a typical time history response captured during the bending test. The initial accelerations at the beginning of the test captured the motion of the hose as it was displaced manually with the rod. After the rod was released, the hose oscillated back to its nominal position with a decaying sinusoidal response. The stiffness and damping of the hose in bending are related to the frequency and rate of decay of the sinusoidal response to the input.

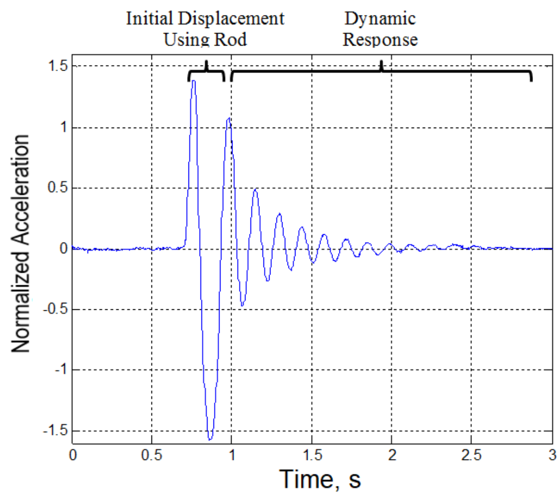

Fig. 4 Normalized acceleration time history of typical hose bending test

Fig. 5 displays an example of the time history of both accelerometers' z-direction outputs to capture the axial behavior. In the case of axial stiffness and damping, one set of experiments was conducted, since there was not a straightforward option to suspend the thermal chamber from the mounting structure.

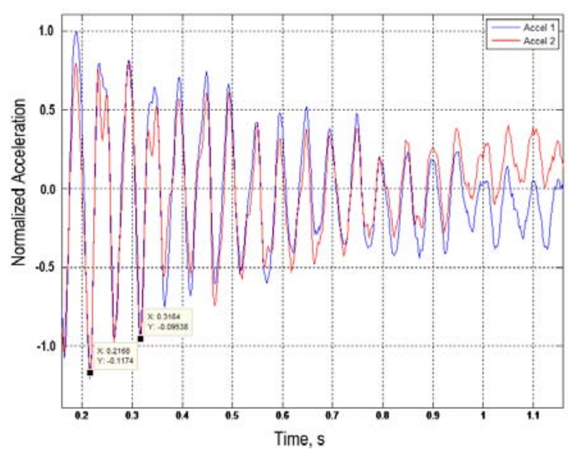

Fig. 5 Example of z-direction acceleration time history response for typical axial test

The bending test results were post-processed to obtain the frequencies of the hose response and the damping for the range of test temperatures. There were a total of 18 bending experiments (three experiments for each temperature). A Fast Fourier Transform (FFT) was performed on each test and the natural frequency was obtained. The logarithmic decrement method was used to find the bending damping coefficient. The frequency and damping coefficients obtained for a given temperature were averaged to obtain a single coefficient corresponding to each temperature.

Fig. 6 shows the normalized frequency squared (which is proportional to stiffness) and the normalized damping coefficient for bending cases as a function of temperature. The experimental values are presented in the plot as circled dots. The figures demonstrate the significant temperature dependence of the hose structural properties.

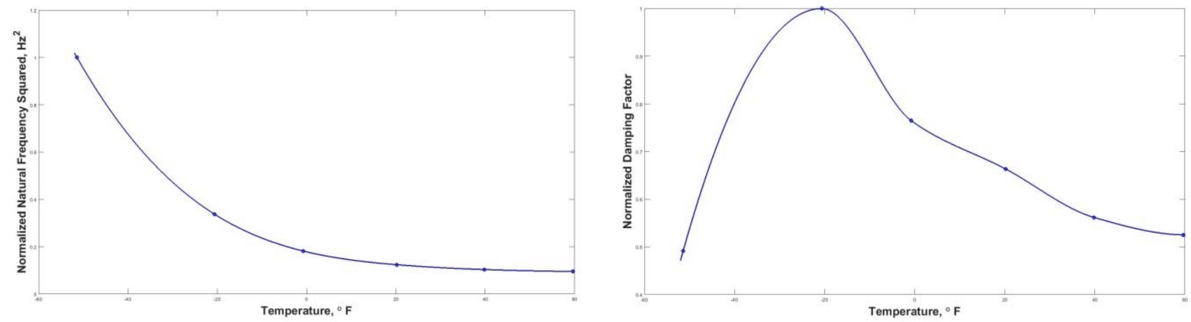

Fig. 6 Normalized lateral frequency squared and damping coefficient vs temperature

The hose bending stiffness and damping coefficients, and axial stiffness and damping coefficients, were tuned to match the frequencies and damping values of the test results. The stiffness and damping data used in the model is summarized in Fig. 7. The number of elements defines the element length used in the simulation of the hose experiment. The shorter the element, the stiffer and more damped each element becomes to represent the same characteristics of the hose as a whole.

The circles in the figures below indicate the processed test data points for each element length. Values between the points are interpolated by a cubic spline curve fitting method. A two dimensional lookup table based on the hose length and temperature was created for the hose stiffness and damping coefficients. The normalized stiffness and damping lookup table data points are shown in Fig. 7, along with the temperature interpolation curves. This approach allows for stiffness and damping values to be interpolated for any length hose element at any temperature. This provides flexibility in discretizing the full aerial refueling hose to allow the choice of hose element length to balance computational accuracy with efficiency.

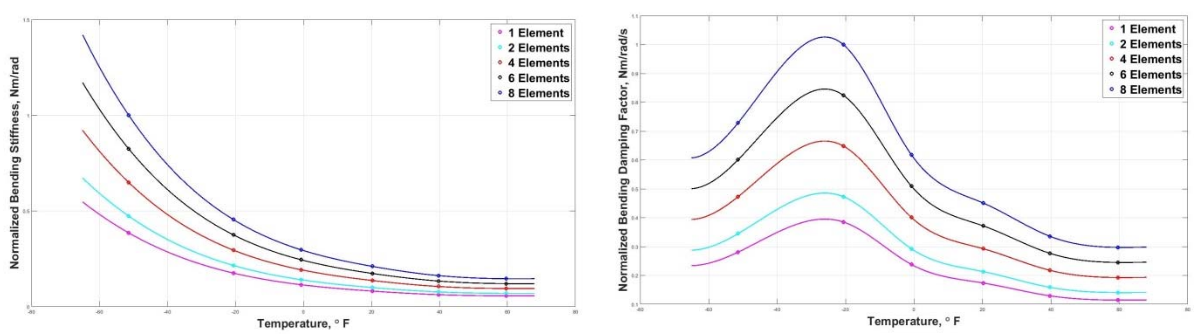

Fig. 7 Hose element normalized bending stiffness and damping for simulation model

A similar procedure was used for the axial stiffness and damping coefficients. It is assumed the bending and axial parameters change proportionally with respect to the hose temperature. From the hose bending experiment, the ratios between the stiffness and damping values at each test temperature and the room temperature test were calculated. These ratios were used to extrapolate the axial stiffness and damping values across the range of temperatures based on the values from the room temperature test.

C. Hose Aerodynamic Model

The hose analysis presents a nonlinear aeroelastic problem, with large hose deflections primarily driven by aerodynamic loads. The hose aerodynamic forces are calculated using Jorgensen's Formulas of slender body theory and each hose element is treated as an inclined cylinder in the airstream (Ref. [4]). Let the element have length L, and reference area A_r. For lift in the element's local z-direction, the reference area is the frontal projected area. For drag along the element's local x-direction, the reference area is the wetted area. The x-direction of the element's local axes points along the centerline of each cylindrical element. The body travels at a speed, U, and at an angle of attack, α. The normal and axial force components are defined as follows:

$$F_N = \frac{1}{2}\rho U^2 C_N A_r \tag{3}$$

$$F_A = \frac{1}{2}\rho U^2 C_A A_r \tag{4}$$

where:

$$C_N = \frac{A_b}{A_r}\sin 2\alpha \cos\frac{\alpha}{2} + \frac{A_p}{A_r}C_{dn}\sin^2\alpha \tag{5}$$

$$C_A = C_{A0}\cos^2\alpha \tag{6}$$

A_p is the planform (projected) area and A_b is the stern base area. For the special case of a cylinder, $A_b = A_p$. At a specific Reynolds number, given by $Re = U \sin\alpha\, D/v$, the crossflow drag coefficient, C_{dn}, is given by

$$C_{dn} = \begin{cases} 1.2 \quad , & Re < 3\times10^5 \\ 0.3 \quad , & 3\times10^5 < Re < 7\times10^5 \\ 0.6 \quad , & 7\times10^5 < Re \end{cases} \tag{7}$$

where D is outer diameter of circular cross-section and v is kinematic viscosity. The axial drag coefficient, C_{A0}, accounts for both friction and form drag. C_{A0} ranges from 0.002 to 0.006 for slender streamlined bodies based on the wetted surface area and on $Re = U L_c/v$, where L_c is $\pi r/\sin\alpha$ and r is the radius of the circular cross-section.

Hoerner's experimental data for a circular cylinder was used to estimate the skin friction and pressure drag of the hose. In the range of the flight operation envelope and the hose size of aerial refueling, the pressure drag is $C_{dn} = 1.2$, and the skin friction is $C_{A0} \approx 0.004$. Since the hose length is much longer than its diameter, the first term in Eq. (5) vanishes.

As the hose elements are moving in the dynamic simulations, the airspeed U and the angle of attack α in the above formulas should account for the local velocity of the element center. The resultant nonlinear element loads depend on element rotation and velocities. The local velocity is added against the normal and axial component of the airspeed, thus the normal and axial drag equations become:

$$C_N = \frac{A_p}{A_r}C_{dn}\left(\sin\alpha - \frac{w}{U}\right)^2 \tag{8}$$

$$C_A = C_{A0}\left(\cos\alpha - \frac{u}{U}\right)^2 \tag{9}$$

where u and w are the tangential and normal components of local velocity, respectively.

D. Drogue Model

A basic diagram of the drogue model is shown in Fig. 8.

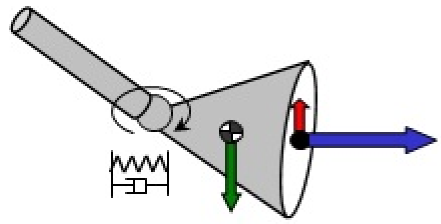

Fig. 8 Simscape Multibody drogue model illustration

The connection between the hose and the drogue is modeled as a ball-hinge joint that freely rotates between ±22.5°. The bending moment depends nonlinearly on the relative rotation angle; it is zero within the free-play zone to represent free rotation about the hinge, and outside this zone it is proportional to the angle multiplied by a large penalty stiffness. Damping and friction may also be added to the drogue joint. The aerodynamic drag and lift on the drogue are given by:

$$D = \frac{1}{2}\rho U^2 C_D A \tag{10}$$

$$L = \frac{1}{2}\rho U^2 C_L A \tag{11}$$

The drag force is applied at the center of pressure in the direction of the free stream while the lift force is applied perpendicular to the free stream. The lift and drag coefficients and projected frontal area *A* were chosen to match the experimental data of the drogue drag.

E. Hose Reeling Model

For aerial refueling with a hose-and-drogue system, steady hose tension is maintained using a hose reeling mechanism. In the reeling mechanism, excess hose is wound around a drum that is driven by either a hydraulic system or an electric control system. As slack develops in the hose, the hose tension drops, which allows the system to wind excess hose onto the drum. As the hose tension increases, the system lets out the hose, keeping the tension within the desired range (Ref. [6]). The angular acceleration of the hose reel drum is given by:

$$\ddot{\theta} = \frac{T_{Reel} - F_{Hose} \cdot R_{Reel}}{I_{Reel}} \tag{12}$$

where T_{Reel} is the torque provided by the reeling mechanism and is dependent on the specific system used, F_{Hose} is the tension in the hose at the entrance to the reeling mechanism, R_{Reel} is the radius of the hose reel, and I_{Reel} is the moment of inertia of the hose reel drum. It should be noted that R_{Reel} and I_{Reel} vary as the hose is wound onto and off of the drum. SDI has developed a simple model of the hose reel system in which the torque provided by the system is simply prescribed rather than calculated using a detailed model of either the hydraulic or electric systems.

IV. Model Verification and Validation

The following model verification and validation exercises have been performed to ensure the accuracy of the hose modeling approach.

A. Verification of Structural Model

Simscape Multibody models of the bending tests using eight hose elements were run with the calculated stiffness and damping values. The natural frequency and damping factor results are presented in Fig. 9. These natural frequencies and damping factors computed from the simulation results showed excellent agreement with the test results, with all calculated values within 1.5% of the test data.

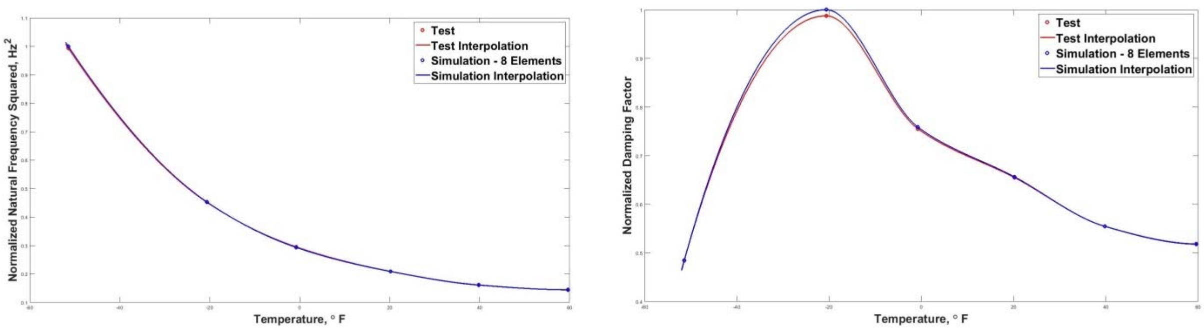

Fig. 9 Normalized lateral frequency squared and damping coefficient vs hose temperature

B. Flight Test Comparisons

In order to begin validation of the complete ARES model, NAVAIR provided several flight test data sets, which included different configurations of tanker aircraft, reeling mechanism type, hose and drogue type, and receiver aircraft.

1. Drogue Response to Tanker Pitch Doublets

NAVAIR conducted flight tests using a F/A-18 “Buddy Store” pod mounted to the underside of the fuselage of a modified Calspan G-III business jet. The configuration is shown in Fig. 10. The original purpose of these tests was to evaluate the capability of an Optical Reference System (ORS) used to calculate the relative positions of the drogue and receiver probe during refueling with the eventual goal of enabling autonomous aerial refueling. During the flight tests, the drogue was excited via aircraft pitch-doublet maneuvers in which the aircraft pitch is quickly increased and then decreased from the level-flight pitch angle. Because the hose and drogue tow point is aft of the aircraft center of pressure, the pitch doublet maneuver produces a vertical sinusoidal motion of the hose tow point, which in turn excites vertical motion of the hose and drogue. The drogue vertical motion was captured by the ORS and can be used as a comparison to the ARES simulation results.

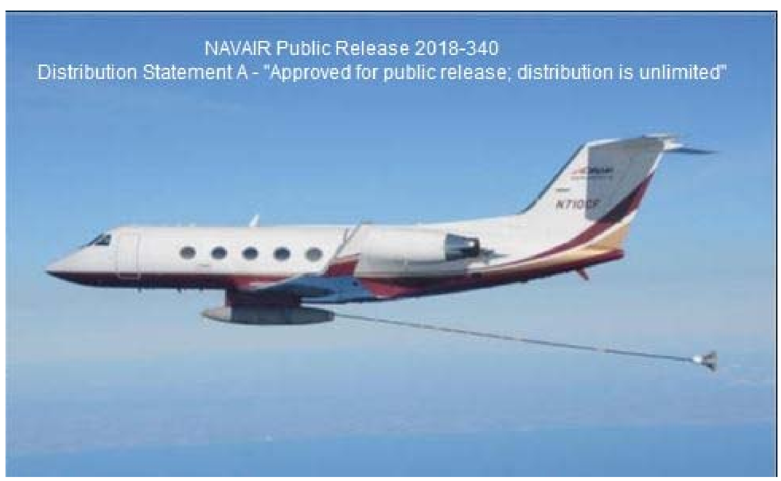

Fig. 10 NAVAIR Calspan G-III with Buddy Store refueling system

In the ARES simulation, the vertical motion of the tanker tow point was prescribed and the hose and drogue responses were simulated. Simulations using the calculated hose aerodynamic forces and drogue drag force compared favorably with flight test data. However, the simulation results appear to be highly dependent on the drogue lift force. The steady-state hose trail position measured in the flight test data indicates the drogue experiences far less lift than was measured in wind tunnel tests. NAVAIR previously conducted a wind tunnel test of the F/A-18 drogue and determined the drag and lift coefficients and frontal area, as used in Eqs. 10 and 11. ARES was run, with and without drogue lift included, and the time-history of the simulated drogue response was compared to the flight test results and NAVAIR’s existing hose model as shown in Fig. 11.

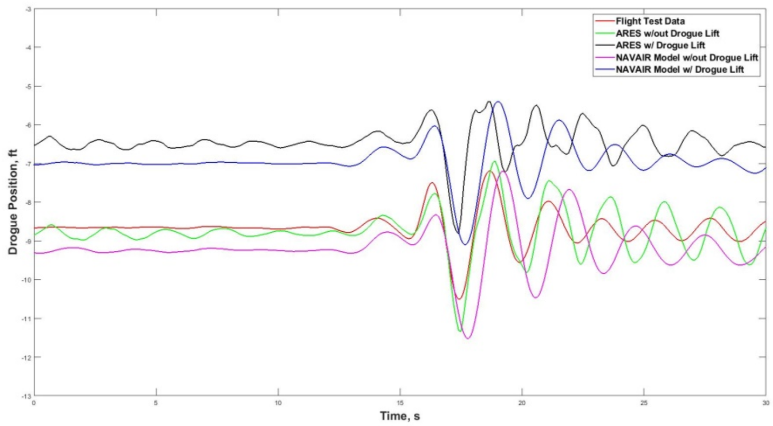

Fig. 11 Comparison of drogue response to tanker pitch doublet

All models show similar dynamic responses with the steady-state drogue position being the largest difference between models. The ARES model without drogue lift aligns closest with the steady state drogue position, but exhibits slightly larger amplitude of oscillations in response to the tanker pitch doublet. All models show similar frequency and damping. The fundamental frequency of oscillation of the flight test data and each model was calculated by FFT; Table 1 shows the fundamental frequency for each case. The models including drogue lift experience slightly higher frequency oscillation, while the models neglecting drogue lift experience slightly lower frequency oscillation than the flight test data.

Table 1 Fundamental frequency for drogue response cases

Model	Drogue Frequency (HZ)
Flight Test Data	0.411
ARES without drogue Lift	0.404
ARES with drogue Lift	0.472
NAVAIR model without drogue lift	0.341
NAVAIR model with drogue lift	0.394

The drogue lift coefficient has a significant effect on the steady-state trail position of the drogue, as well as the drogue dynamic response to tanker maneuvers. With drogue lift included, the steady-state vertical position of the drogue below the tanker attachment point is too high. Neglecting drogue lift brings the drogue position in line with the flight test data. Boothe et al found similar difficulty in correlating measured wind-tunnel drogue lift with real-world flight test results (Ref. [7]). One possibility is that the drogue behaves differently in the wake of the G-III aircraft than in the free-stream airflow idealized by the wind tunnel test. Additionally, any wake effects on the drogue from the G-III aircraft are probably significantly different from the F/A-18 wake effects due to the substantially different aircraft fuselage shapes, as well as a difference in tow point on the aircraft. Further investigation into the drogue aerodynamic behavior during refueling scenarios is recommended.

2. Steady-State Hose Trail Position

NAVAIR also provided flight test data for several aerial refueling engagements of an Omega Refueling Services KDC-10 Tanker with an F/A-18 receiver. This tanker utilizes wing-mounted refueling pods similar to the refueling pods used on the KC-130. NAVAIR conducted 11 engagements at similar altitudes and airspeeds but over a range of receiver closure speeds. Videos of the engagements were recorded from a chase plane and from the cockpit of the receiver aircraft. A view of the tanker, hose, drogue, and receiver is shown in Fig. 12.

Fig. 12 Hose equilibrium position behind Omega tanker prior to engagement number 7

The hose position time history data were then derived from the flight test video for four of the events. The four engagements listed in Table 2 were used in the validation of the ARES hose model aeroelastic properties.

Table 2 ORS engagement flight conditions

ORS Engagement	Altitude (ft)	Airspeed (KCAS)	Closure Rate (kts)
7	15050	254	3.89
8	15031	255	4.75
9	15029	255	4.73
11	15012	258	5.25

The Omega KDC-10 tanker uses a “long hose” with a nominal length of 75 feet trailed from a wing-mounted pod. Cobham produces the refueling system, but it is not the same hose as used on the KC-130. Because the structural properties of this hose have not been determined, it was assumed that similar construction to the KC-130 hose would yield similar stiffness and damping properties. These properties were scaled by the ratio of moments of inertia of the respective hoses to compensate for differences in the structural properties of the two hoses. The same aerodynamic coefficients were used for both hoses, with decreased values of cross-sectional area to represent the smaller dimensions of the Omega hose.

The steady-state trail position of the refueling hose was considered first. The steady state hose positions in the four engagement cases are not all consistent. As shown in Fig. 13, engagements 7 and 11 have very similar steady-state trail positions, however, engagements 8 and 9 exhibit very different trail positions despite similar altitudes and airspeeds. Further investigation is required to determine whether this is a result of aerodynamic effects that are unaccounted in the current model. The ARES model currently uses altitude, airspeed, hose position and the relative wind velocity to calculate the lift and drag on the hose and drogue. Additional aerodynamic effects that are planned for integration into the ARES model include tanker wake effects, turbulence, receiver bow wave effects, steady-state wind, turbulence and gusts, and three-dimensional aerodynamic effects on the hose.

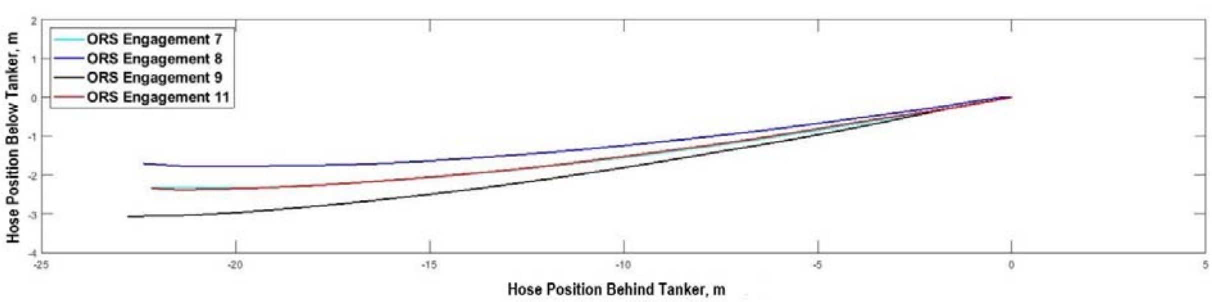

Fig. 13 Comparison of steady-state hose equilibrium position for four ORS engagement cases

Engagements 7 and 11 were used as validation cases for the ARES model and the steady-state trail positions are shown in Fig. 14 and Fig. 15. Again, the drogue lift has a significant effect on the steady-state trail position of the hose and drogue. Because the Omega tanker uses wing-mounted pods and a long hose, the tanker wake effects seem to be smaller than for the fuselage mounted hose and drogue. For these cases, neglecting drogue lift resulted in a trail position that was lower than the test data, and using the wind-tunnel measured lift resulted in a trail position too high. Therefore, the lift coefficient was tuned to produce the correct drogue vertical position, with the same value used for both engagement cases 7 and 11. Because the lift coefficient has been tuned, the comparison to the flight test data is a validation of only the hose structural properties and aerodynamics. Both cases 7 and 11 show very good agreement with the flight test data across the length of the hose.

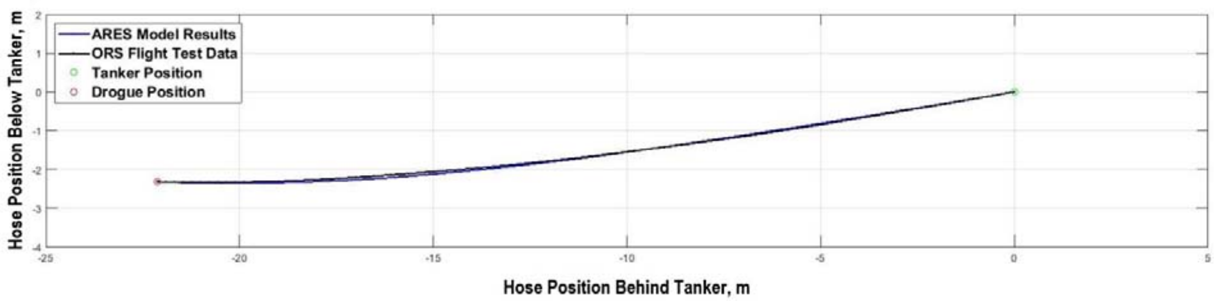

Fig. 14 Steady-state equilibrium comparison of ARES model and ORS engagement 7 flight test data

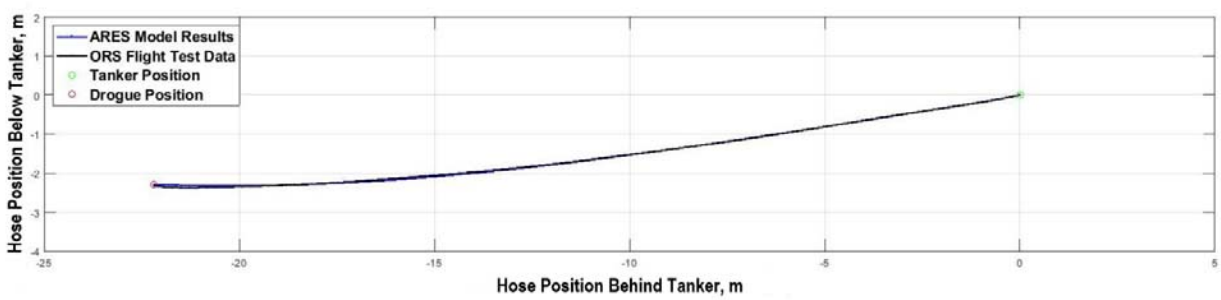

Fig. 15 Steady-state equilibrium comparison of ARES model and ORS engagement 11 flight test data

V. Results and Discussion

The hose model was also used to analyze several complete aerial refueling engagement events.

A. Hose Reeling System Behavior

A simple investigation of the hose reel system effects on the hose whip behavior was conducted. In a serious hose whip event, the hose tension drops after the receiver-drogue contact, allowing slack to develop in the hose This increases the angle of attack of the hose, which increases the lift and drag forces and induces a traveling wave "whipping" motion. This produces loads that may cause the drogue to disconnect from the probe or even damage the drogue and probe. By removing slack from the hose and regulating the hose tension, the hose reeling system aims to reduce hose whips and the resulting increase in loads (Ref. [6]).

A comparison of the hose behavior during an engagement scenario with and without a hose reel is shown in Fig. 16. On the left side of Fig. 16, the top image shows the development of slack, the middle image shows the subsequent development of a traveling wave, and the bottom image shows the wave impacting the probe. The right side of Fig. 16 shows the hose position resulting from the same engagement scenario with the functioning hose reel and the effective prevention of a hose whip. The results in Fig. 16 with reeling were generated with the simplified hose reel, which maintains steady hose tension by simply prescribing the hose tension at the tanker as equal to the initial steady-state hose tension. It therefore represents an idealized case of the hose reel, in which the dynamics of the reeling drum are not considered; however, it demonstrates the significant effect the hose reel system has on the hose dynamics during engagement.

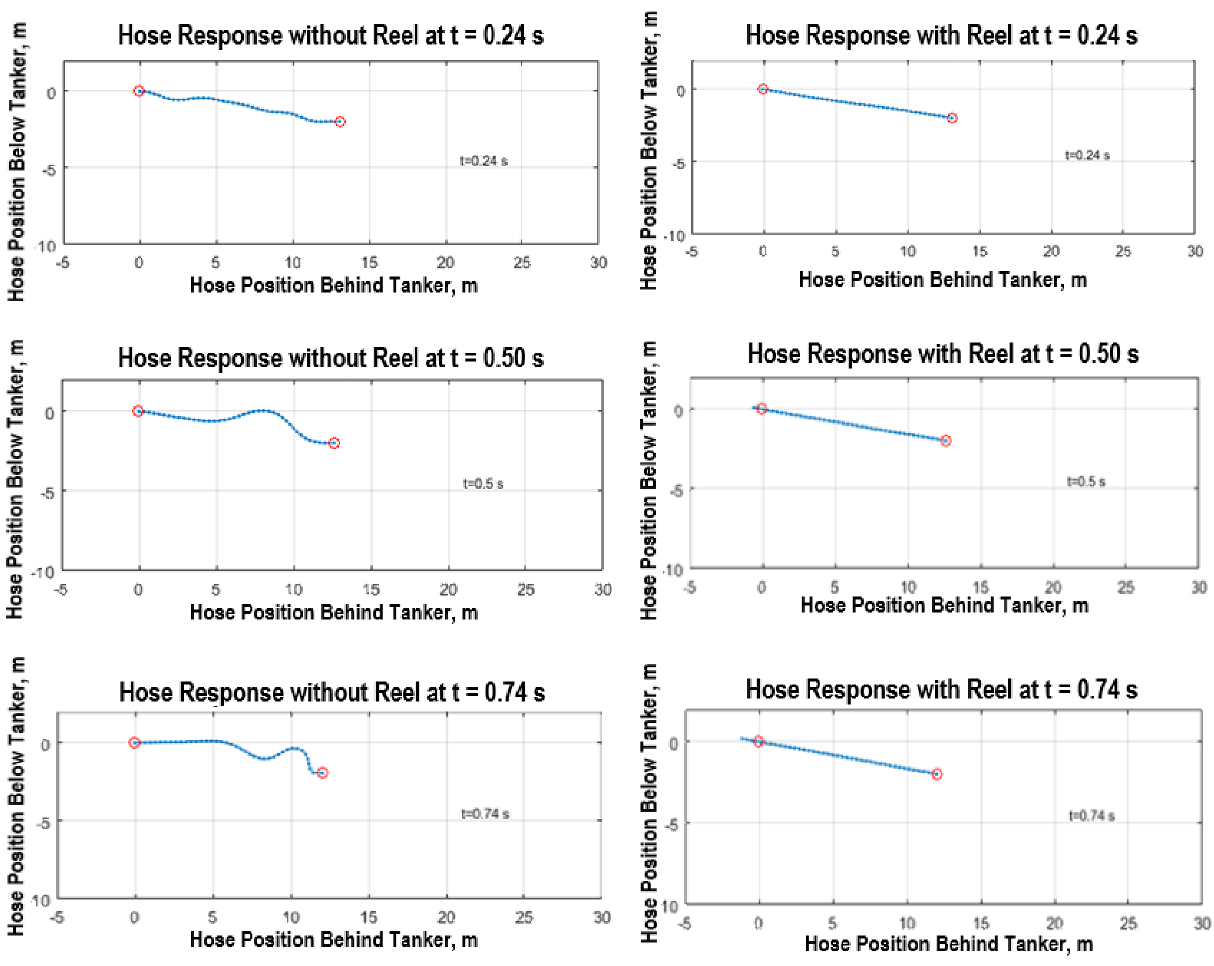

Fig. 16 Comparison of hose response with and without reeling mechanism after probe-drogue engagement

B. KDC-10 Hose Response to Receiver Engagement

The NAVAIR flight test data discussed in Section IV.B.2 was also used to investigate the hose dynamic response to receiver engagement and reel uptake. The complete ORS Engagement 7 as described in Table 2 was simulated using ARES. For this comparison, only the aeroelastic effects of the hose were considered, with the boundary conditions chosen to match the flight test data. For the hose reel response, the length of hose inside the reel was derived by calculating the length of hose absent from the flight test data at each time step. This effective hose reel position is shown in Fig. 17 and was prescribed during the simulation. The drogue fore-aft and vertical positions were calculated from the flight test data as shown in Fig. 18 and prescribed to the drogue model. Once the receiver's probe has connected with the drogue, the drogue position is purely a function of the probe position. Any drogue lift and drag is simply carried by the probe and no longer affects the drogue's position or the hose dynamics. Note that the hose reel response is very similar to the change in the x position of the drogue, however, the hose reel motion exhibits an approximate 0.2 second delay relative to the drogue's motion.

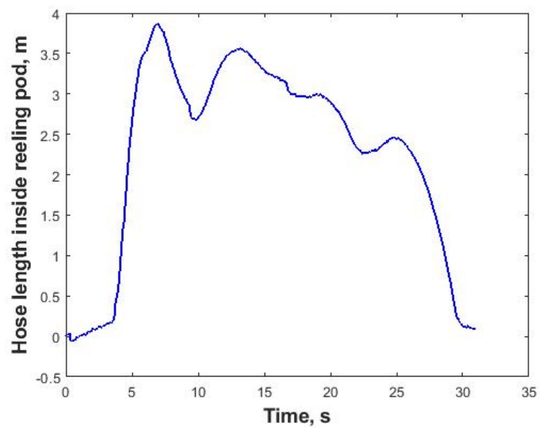

Fig. 17 Length of hose taken up by hose reel pod during ORS engagement 7

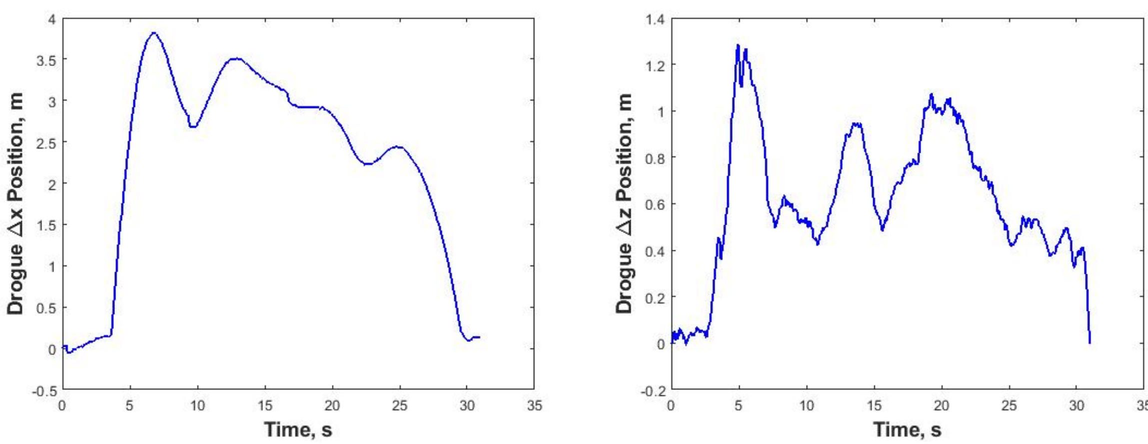

Fig. 18 Change in drogue X and Z position from initial steady-state equilibrium position during ORS engagement 7

The progression of the hose position throughout the aerial refueling process is shown in Fig. 19. The first image shows the hose position at the time of the probe-drogue contact. The second image shows the development of slack in the hose before the reel can respond to the reduction in hose tension. The simulation accurately captures the overall hose position as well as the development of larger curvature close to the drogue; however, the hose-drogue connection joint does not experience as much rotation in the simulation as in the flight test. Detailed modeling of the hose-drogue connection joint and probe-drogue coupling is likely necessary to capture the complicated dynamics and large deflections occurring in this location.

The third image shows the maximum slack developing, and a transverse wave beginning to travel up the hose toward the tanker. The fourth image shows the time of maximum hose reel uptake and the reduction of the traveling wave as the hose tension is regulated. In the fifth image, the receiver aircraft has slowed to match the airspeed of the tanker and is in the zone behind the tanker where refueling may commence. The hose length and tension has stabilized and the hose reaches a new steady-state equilibrium position. In the final image, the receiver aircraft begins to slow and back away from the tanker, and the hose reel feeds out the hose until the maximum hose length is reached, and the probe disconnects from the drogue.

Throughout the complete aerial refueling process, the ARES model hose dynamics correlates well with the flight test data. Thus far, the comparison between the flight test dynamic hose response and the model results has been qualitative. Future validation work includes measuring the speed of the transverse wave induced by the probe-drogue contact, and calculation of the loads induced on the probe over the course of the refueling event.

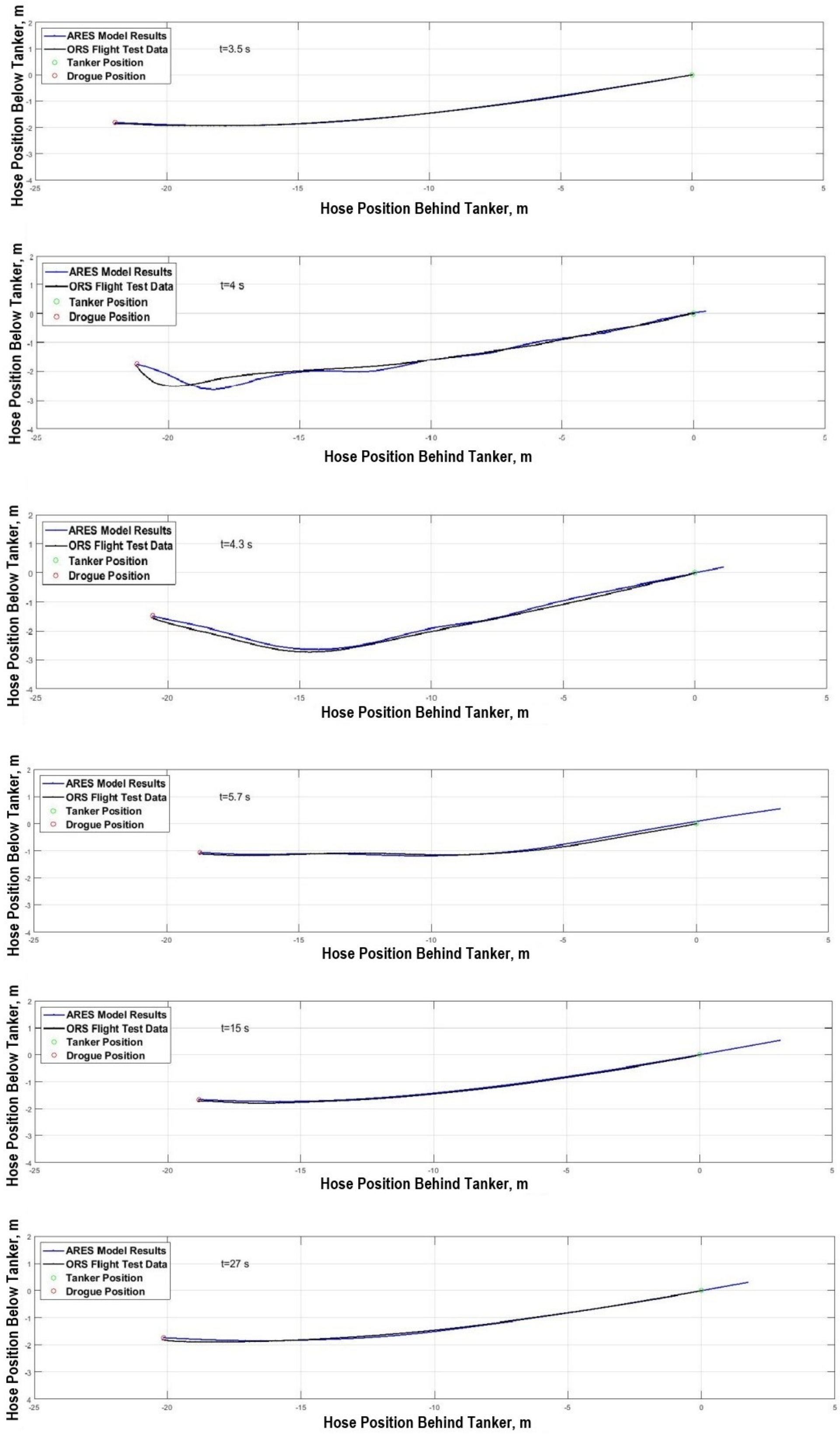

Fig. 19 Progression of hose and reel response to receiver engagement

VI. Conclusion

In this paper, the ARES software has been introduced. The basic theory and equations behind the aerial refueling hose, drogue, and reeling models have been described. Validation and verification exercises were also presented, including comparisons to NAVAIR's existing hose model as well as available flight test data. Overall, the ARES model results compare well against the flight test validation cases and NAVAIR's existing model results for both quasi-static and dynamic cases. The hose reeling system has also been shown to be very effective at reducing hose whip. This agrees with anecdotal evidence from NAVAIR that suggests probe failures are rare and are often the result of excessive receiver closure speed or reel system malfunction.

Challenges in accurately modeling the complete aerial refueling process were discussed. The static and dynamic hose and drogue behavior were found to be highly dependent on the drogue lift. The drogue lift measured in wind tunnel tests also did not correlate well with flight test results. This highlights the need for further investigation of the drogue aerodynamic characteristics, the consideration of additional aerodynamic effects, and the inclusion of an accurate tanker wake model.

Future areas of work that SDI plans to complete as part of future ARES development include extending the model to three dimensions and including unsteady aerodynamics, tanker wake effects, receiver bow-wave effects, probe-drogue engagement modeling, and modeling of the hydraulic and electric reeling systems. ARES will then be used to investigate hose, drogue, and probe loads during all phases of aerial refueling operations. As part of this effort, SDI will further develop the probe-drogue contact model and probe structural model.

Acknowledgments

SDI Engineering would like to thank NAVAIR for their support of the ARES development and validation effort through the SBIR program. This material is based upon work supported by the United States Navy under Award No N68335-18-C-0026. Any opinions, findings, and conclusions or recommendations expressed in this publication are those of the author(s) and do not necessarily reflect the views of the United States Navy or SDI Engineering Inc.

SDI thanks Steve McLaughlin and Elizabeth Knoblauch for their encouragement of industry collaboration and their commitment to the advancement of aerial refueling modeling and simulation. SDI thanks Dr. Marat Mor for his assistance in developing the hose reel model and conducting model validation cases.

References

[1] Zhu, Z.H., Meguid S., "Modeling and Simulation of Aerial Refueling by Finite Element Method," *International Journal of Solids and Structures*, 44, pp. 8057-8073, 2007.

[2] Burgess, J.J., "Equations of motion of a submerged cable with bending stiffness," *Offshore Marine and Arctic Engineering*, 1-A, 283–289, 1992.

[3] Howell, C.T., "Numerical analysis of 2-D nonlinear cable equations with applications to low-tension problems," *Int. J. of Offshore and Polar Engineering*, 2, 110–113, 1992.

[4] Ribbens, W., Saggio, F., Wierenga, R., and Feldmann, M., "Dynamic Modeling of an Aerial Refueling Hose & Drogue System," *25th AIAA Applied Aerodynamics Conference*, Miami, FL, 25-28 June 2007.

[5] Boothe, K., Koehler, E., Vess, R., Knoblauch, E., and McLaughlin, S., "An Introduction to the Navy's Physics Based Model of the Hose and Drogue Refueling System – Design and Validation," *AIAA Modeling and Simulation Technologies Conference,* Kissimmee, Florida, January 8-12, 2018.

[6] Hoerner, S.F., *Fluid-Dynamic Drag*, Hoerner Fluid Dynamics, NJ, 1985.

[7] Vassberg, J.C., Yeh, D.T., Blair, A.J., and Evert, J.M., "Numerical Simulations of KC-10 Wing-Mount Aerial Refueling Hose-Drogue Dynamics With A Reel Take-Up System," AIAA Paper 2003-3508, June 2003.